

Identification of single nucleotides in MoS₂ nanopores

Jiandong Feng^{1#}, Ke Liu^{1#}, Roman D. Bulushev¹, Sergey Khlybov¹, Dumitru Dumcenco², Andras. Kis², Aleksandra Radenovic^{1*}

¹ *Laboratory of Nanoscale Biology, Institute of Bioengineering, School of Engineering, EPFL, 1015 Lausanne, Switzerland*

² *Laboratory of Nanoscale Electronics and Structure, Institute of Electrical Engineering, School of Engineering, EPFL, 1015 Lausanne, Switzerland*

**correspondence should be addressed to aleksandra.radenovic@epfl.ch*

equal contribution

ABSTRACT

Ultrathin membranes have drawn much attention due to their unprecedented spatial resolution for DNA nanopore sequencing. However, the high translocation velocity (3000-50000 nt/ms) of DNA molecules moving across such membranes limits their usability. To this end, we have introduced a viscosity gradient system based on room-temperature ionic liquids (RTILs) to control the dynamics of DNA translocation through a nanometer-size pore fabricated in an atomically thin MoS₂ membrane. This allows us for the first time to statistically identify all four types of nucleotides with solid state nanopores. Nucleotides are identified according to the current signatures recorded during their transient residence in the narrow orifice of the atomically thin MoS₂ nanopore. In this novel architecture that exploits high viscosity of RTIL, we demonstrate single-

nucleotide translocation velocity that is an optimal speed (1-50 nt/ms) for DNA sequencing, while keeping the signal to noise ratio (SNR) higher than 10. Our findings pave the way for future low-cost and rapid DNA sequencing using solid-state nanopores.

Keywords: Molybdenum disulfide (MoS₂), deoxyribonucleic acid (DNA), solid-state nanopores, single molecule, ionic liquids, DNA sequencing

INTRODUCTION

Translocation velocity of DNA molecules in solid-state nanopores is on the order of 3000-50000 nt/ms¹. This large translocation velocity range originates from different parameters such as the wide range of the pore sizes (1.5-25 nm) and applied potentials (100 mV-800 mV)¹.

The high translocation velocity of DNA molecules, together with a low ionic current signal-to-noise ratio and a relatively large sensing region due to the pore membrane thickness, that is typically 10 -20 nm and therefore can accommodate 30-60 nucleotides at a time¹, has been a major obstacle for achieving sequencing data in solid state nanopores. Although single nucleotide identification^{2,3} and DNA sequencing using biological pores have already been demonstrated^{3,4} their fragility, difficulties related to measuring pA-range ionic currents together with their dependence on biochemical reagents, make solid state nanopores an attractive alternative⁵. In contrast to bio-engineered pores, solid state nanopores can operate in various liquid media and pH conditions, their production is scalable and compatible with nanofabrication techniques and does not require the excessive use of biochemical reagents. All these advantages are expected to lower the cost of sequencing. The basic sensing principle is the same as in bio-engineered pores. Ideally, the sequence of nucleotides, genetic information, along a single DNA molecule can be registered by monitoring small changes in the ionic current caused by the transient residing of single nucleotides within a nanometer-size pore⁶. In addition, solid state nanopores allow a transverse detection scheme, based on detecting changes in the electrical

conductivity of a thin semiconducting channel caused by the translocating molecule. The DNA translocations in biological nanopores are currently too slow, on the other hand in solid-state nanopores are too fast compared to the optimal DNA sequencing velocity of 1-50 nt/ms⁷.

Achieving optimal translocation speed for both biological and solid state nanopores remains a significant challenge⁸⁻¹⁸. Here, we demonstrate that molecular translocation speeds in a nanopore sensing system can be decreased by two to three orders of magnitude using an ionic liquid/water viscosity gradient system together with a nanopore fabricated in atomically thin membranes of molybdenum disulfide (MoS₂) which fulfil the requirement for spatial resolution. This requirement has been first met with the graphene membranes¹⁹⁻²¹. By using graphene, the thinnest known material, the ultimate end thickness of the membrane for solid state nanopores has been reached¹⁹⁻²¹. Nanopores realized in three-layer graphite structures having thickness of 1 nm should display higher signal to noise ratio compared to single –layer graphene nanopores^{22,23}. The use of 2D materials such as graphene is particularly interesting since it allows concomitant detection of DNA translocation with two synchronized signals, i.e., ionic current in the nanopore and the current in the graphene nanoribbons (GNR) as recently demonstrated by our group⁵. However, pristine graphene nanopores exhibit strong hydrophobic interactions with DNA²⁴ that limit their long-term use due to clogging, requiring the use of surface functionalization^{25,26}. In parallel, other 2D materials, such as boron nitride (BN)²⁶ and MoS₂²⁷ have been implemented

as alternatives to graphene while fabrication advances allowed for realization of nanopores in ultrathin SiN_x ²⁸ and HfO_2 ¹⁸. MoS_2 nanopores are particularly interesting since they can be used for extended periods of time (hours even days) without any additional functionalization²⁷. Sticking behaviour of DNA to MoS_2 nanopore is reduced due to the Mo-rich region around the drilled pore after TEM irradiation²⁹ while the stability could be attributed to its thickness.

Single-layer MoS_2 has a thickness of 0.7 nm and a direct band gap of at least 1.8 eV^{5,30} which is essential for electronic base detection in field-effect transistors (FETs)^{5,31} thus making MoS_2 a promising material for single-nucleotide detection, as recently computationally demonstrated by Farimani *et.al.*³²

Our approach to slow down DNA translocation, has been inspired by the remarkable physical and chemical properties of RTILs, non-aqueous electrolytes composed of a pair of organic cations and anions. RTILs have been termed “magical chemicals”, due to the high degree of freedom in fine-tuning their structure that allows tailoring physical and chemical properties for a given application³³. We have chosen 1-butyl-3-methylimidazolium hexafluorophosphate (BmimPF_6), since it has a broad viscosity window of 10-400 cP³⁴, which can be tuned to optimize the temporal resolution. Tunability can be obtained either by varying the temperature (20°C-50 °C) or by mixing BmimPF_6 and BmimPF_4 in different ratios³⁵. BmimPF_6 is also a friendly solvent for bio-molecules and most importantly, it exhibits good ionic conductivity of 1.4 mS cm^{-1} ³⁴. It has also been widely used as an electrolyte with a wide

electrochemical window³⁶. In contrast, the low conductivity of glycerol limited previous attempts to a narrow viscosity window (1.2-5 cP) and consequently achieved only modest improvement in DNA translocation speed (3000 nt/ms)⁸. In our viscosity gradient system, schematically shown on **Fig. 1a**, it was possible to employ pure BmimPF₆ without compromising the conductance of the MoS₂ nanopore for all tested nanopore devices listed in SI Table 2. Details on the properties and fabrication of MoS₂ nanopores can be found in Methods section of this paper and in Liu *et al.*²⁷

For example even in the large nanopore 17 ± 2 nm conductance in pure RTILs is relatively low (~ 1 nS)³⁷ when compared to KCl, **Fig. 1c**, inspired by the use of concentration gradient systems in nanopores³⁸, we have realized a viscosity and concentration gradient system with the conductivity of 210 nS. The *cis* chamber in our system contains RTILs (BmimPF₆) while *trans* chamber contains 2M aqueous KCl solution. It is important to note that here we use two types of solvents with completely different physicochemical properties and that in the region inside and close to the pore we have in fact a non-homogeneous phase solution. The conductance of 280 nS measured in 2M KCl/2M KCl is reduced to 210 nS in our viscosity gradient system as shown in **Fig. 1c**. To gain insight into the ionic transport through the nanopores in the presence of an inhomogeneous phase solution, we have performed finite element analysis by solving the Poisson–Nernst–Planck (PNP) equation. **Fig 1.d.** shows the mass fraction of water molecules, anions and cations as a function of distance from the nanopore at a transmembrane bias voltage of 400 mV. The sub-nanometer

membrane thickness ensured that a relatively high number of water molecules diffused from the *trans* into the *cis* chamber. Similarly, anions and cations diffused into their respective chambers. Modeled conductances for 2.5 nm, 5 nm 10 nm pore, shown in **SI Fig. 1.d-f**, are in good agreement with our measurements (**SI Fig. 1.a-c**). Interestingly, the mass fraction of water molecules in the *cis* chamber shows a weak dependence on the transmembrane bias, while PF_6^- diffusion is strongly affected (**SI Fig. 1.g**). Having successfully built and characterized our viscosity gradient system, we performed our first translocation experiment by adding 48.5 kbp λ -dsDNA to the *cis* chamber filled with BmimPF₆. In order to minimize the contribution from the nanopore-DNA interaction that can also significantly slow down DNA translocation²⁸, we decided to first use MoS₂ nanopores with relatively large diameters (~20 nm, **SI Fig. 2.a**). Fig. 2a displays the typical current trace recorded during the translocation of the λ -DNA molecule in the viscosity gradient system in the presence of a transmembrane bias voltage of 400 mV. When compared to a typical current trace acquired in a 2M aqueous KCl solution obtained using the same pore and transmembrane voltage, one can observe temporal improvement and no reduction in the amplitude of the current drop. Unlike other viscous systems for slowing down DNA translocation, signal amplitude has been preserved owing to the conductive nature of RTILs and high concentration of chloride ions inside the pore. The average translocation time is 130 ms for λ -DNA in the viscosity gradient system, and 1.4 ms in the 2M KCl solution presenting two orders of magnitude's improvement.

At this point, in the absence of the electro-osmotic flow (EOF) and charge reduction for a given pore, DNA molecule and bias voltage, we can introduce the retardation factor r (for details see **SI**). We obtain a retardation factor higher than 100 that is predominantly due to the increase in the viscosity in our viscosity gradient system. However, scatter plots and DNA translocation histograms in **Fig. 2b** and **Fig. 2c** reveal a large spread in dwell times that can be attributed to several factors associated with the viscosity gradient system. In reality, EOF, charge reduction as well as long-range hydrodynamic effects and the existence of gradients in the free-energy landscape have to be included in the future model and could result in a more complex dynamics of DNA translocation in the viscosity gradient system than assumed in our simplistic model (presented in **SI**). In addition, it is possible that we have overestimated the value of BmimPF₆ viscosity in the vicinity of the pore. More accurate calculation of the retardation factor should include the effects related to charge reduction and the presence of the EOF³⁹. Due to the negative charges at the surface of MoS₂ membrane and within the pore, the direction of EOF is opposite to the direction of DNA translocations and could result in further slowing down. By comparing translocation traces before, during and after translocation events we see that they all have a similar noise level of 520-540 pA (**SI Fig. 3**). We observe a slight increase of noise during the translocation that can be explained by the fact that DNA interacts strongly with BmimPF₆ via electrostatic interaction between the cationic Bmim⁺ groups and DNA phosphates (P-O bonds)⁴⁰. Because of this electrostatic

interaction and the hydrophobic association between Bmim^+ and bases, DNA molecules can act as carriers for Bmim^+ ions from the *cis* to the *trans* chamber.

In general, the single-molecule DNA translocation process can be viewed as a voltage-driven barrier crossing as shown in **SI Fig. 4 a**. To further explain retardation mechanism, we explore the voltage dependence of pNEB 193 (2700 bp long DNA plasmid) translocation dwell times in the MoS_2 nanopore. The observed power law scaling is consistent with Kramer's theory **SI Fig. 4 a, b**. A free-energy barrier predominately arises from the RTILs and KCl/water interface and includes a change in conformational entropy of the translocating polymer. The threading process across nanopore in a high-voltage regime follows a force balance model detailed in **Supplementary Material**. pNEB is almost 18 times shorter than λ -DNA, however we still observe large retardation when comparing average dwell times recorded at 400 mV, under the condition of viscosity gradient 2 ± 0.5 ms, and 40 ± 10 μ s in the 2M KCl aqueous solution.

To exploit the full potential of our viscosity gradient system, we translocate short homopolymers, poly(dA)₃₀, poly(dT)₃₀, poly(dG)₃₀ and poly(dC)₃₀, through a 2.8 nm diameter pore in single-layer MoS_2 , shown in the TEM micrograph on **SI Fig.2b**. DNA-pore interactions can also increase the translocation time by one order of magnitude¹². The 2.8 nm pore in single layer MoS_2 membrane suspended over smaller opening in the nitride, even without any special pretreatment⁴¹, displays better noise properties with a current RMS of 59 pA at 0mV and 89 pA at 200 mV (as

shown in **SI Fig. 7.**) compared to the pores suspended over larger openings. The noise reduction is achieved by restricting the opening for freestanding MoS₂ membrane to the hole having 100 nm diameter.⁴² Self-organization of certain ionic liquids can be further exploited to reduce 1/f noise in single nanopores as shown by Tessarit *et.al.*⁴³ **Fig.3** shows translocation traces of short DNA homopolymers for periods of 0.5 s and 0.1 s respectively. Four peaks can be clearly distinguished in the histogram of current drops shown in **Fig. 3b**. The density scatter plots shown in **SI Fig. 8a** are useful in revealing the range of the most probable dwell time for the four types of poly-nucleotides at the transmembrane bias voltage of 200 mV. The current traces and histogram of poly(dG)₃₀ homopolymer display two peaks. However, from the poly(dG)₃₀ density scatter plot (**SI Fig 8**) one can easily identify which peak is more probable. Based on the amplitude and temporal signature of the second peak, we believe that it might originate from the G-quadruplex formation⁴⁴. Venta *et al.*²⁸ reported a much faster translocation (20 μ s) of such homopolymers using a 1M Hz amplifier in 1.5 nm pores with high applied voltage (1V). However, high bandwidth amplifier introduced additional noise and high voltage might reduce the lifetime of the device. In the viscosity gradient system and 2.8 nm pore, we achieved 10-50 times slowing down compared to the results from Venta *et al.*²⁸

Finally, using the same 2.8 nm diameter MoS₂ nanopore, we translocate single nucleotides, dAMP, dTMP, dGMP and dCMP. The exceptional durability of the MoS₂ nanopore has allowed us to perform 8 consecutive experiments with high

throughput (more than 10000 events collected, enabling robust statistical analysis) (**Fig. 3** and **Fig. 4**) in the same pore. Each experiment has been preceded with the flushing of the fluidics and with the short control experiment to confirm the absence of the analyte from the previous experiment. Not only does this show the extraordinary resilience of our nanopores, but, to our surprise, the dwell times of single nucleotides are comparable to those of 30mer homopolymers. At this scales, when comparing the dwell times of single nucleotides to homopolymers, one needs to account for the charge reduction difference that will result in the lower net force acting on the single nucleotide compared to the homopolymers. In the pores with diameters $< 5\text{nm}$, observed translocation retardation is a cumulative effect that includes several components: interaction of the translocating molecule with the pore wall, electrostatic interaction between Bmim^+ cations and phosphate groups of DNA, the hydrophobic association between Bmim^+ and DNA bases⁴⁵ and finally, the viscosity gradient. The contribution of the viscosity gradient to the retardation will increase with the increasing DNA length. Consequently, for single nucleotides this contribution is decreased, however due to the charge reduction, the lower net force acting on the single nucleotide might account for observed long translocation times of single nucleotides.

The use of single-layer MoS_2 as the membrane material and the viscosity gradient system in combination with the small nanopore have been crucial for the single nucleotide discrimination as shown in **Fig. 4. SI Fig.9** shows translocation

traces of four single nucleotides for periods of 0.5 s and 0.1 s respectively. Here, the obtained translocation speed is in the range from 1-50 nt/ms. In accordance with the physical dimensions for four nucleotides, we observe for dGMP, centered at 0.8 nA and a smallest current drop for the smallest single nucleotide dCMP, centered at 0.3 nA. These observations are in good agreement with the results obtained on single nucleotide discrimination using protein pores²⁻⁴. Although the current drop for dAMP is slightly larger than dTMP (0.65 nA compared to 0.45 nA), we believe that this inconsistency might be due to the stronger Bmim⁺ affinity towards dAMP compared to dTMP⁴⁶. It has been established that RTILs could selectively bind to DNA⁴⁰, while RTILs based on metal chelate anions could be designed to have specific bonding to the bases⁴⁷. In our system, this could be further exploited to amplify the small differences in bases. Using only ionic current drops of 500-3000 events for four nucleotides, we performed a Welch's t-test and found p-values to be all less than 0.0001. Moreover, this simple statistical analysis revealed a minimum event number to be 6-9 for nucleotide identification with a confidence of 99%. With the addition of the other parameters such as dwell time it might be possible to identify single nucleotides with one read while the presence of a direct band gap in MoS₂ should allow for straightforward multiplexing in a detection scheme based on the transverse current. We have also reproduced the discrimination of single nucleotides in a slightly bigger pore with a diameter of 3.3 nm under the same conditions of the viscosity gradient system (**SI Fig. 10**) and with a similar number of events (>10000).

When translocating single nucleotides (such as dAMP) and increasing the potential (from 200 mV to 400 mV), we have observed increases in the current drop amplitudes as shown on **SI Fig. 11**, further confirming that observed events are indeed from single nucleotide translocation. However, applying a higher potential caused an increase in the noise. The data presented on **SI Fig. 10** and **SI Fig. 12** are therefore collected at 200 mV. As expected, in the 3.3 nm pore, the translocation events (>10000) were faster and produced smaller current amplitude drops compared to the 2.8 nm pore and other smaller pores (**SI Fig. 12**). However, the trend of current drops for different types of nucleotides remained the same, as shown in **Fig 4**. (dGMP>dAMP>dTMP>dCMP). Similarly as we did for the 2.8 nm pore, by performing the Welch's t-test, we found that 14 events are needed for nucleotide identification with 99% confidence. **SI Fig. 12** shows correlation between mean current drops related to four nucleotides and pore sizes. The dashed line placed between 3.5 nm and 4 nm indicates the maximum pore size that still allows nucleotide differentiation. In addition, translocating nucleotides in pores as small as 2 ± 0.2 nm can dramatically increase SNR up to 16.

To conclude, we have demonstrated that single-nucleotide identification can be achieved in MoS₂ nanopores by using a viscosity gradient to regulate the translocation speed. The viscosity gradient system can not only be used in standard ionic sensing experiments but it can be potentially combined with other schemes of nanopore sensing such as transverse current signal detection. The ultrahigh viscosity of ionic

liquids results in reduced capture rates. Therefore, an optimal experimental configuration would capitalize on high-end electronics²⁸ and the viscosity gradient system presented here with a suitable capture rate. We believe that combining ionic liquids and monolayer MoS₂ nanopores, together with the readout of transverse current, either using the tunneling^{48,49} or FET modality^{5,31}, would reach all the necessary requirements for DNA strand-sequencing such as the optimal time resolution and signal resolution in a platform that allows multiplexing, thus reducing the costs and enhancing the signal statistics.

REFERENCES

- 1 Branton, D. *et al.* The potential and challenges of nanopore sequencing. *Nat Biotechnol* **26**, 1146-1153, doi:Doi 10.1038/Nbt.1495 (2008).
- 2 Astier, Y., Braha, O. & Bayley, H. Toward single molecule DNA sequencing: Direct identification of ribonucleoside and deoxyribonucleoside 5'-monophosphates by using an engineered protein nanopore equipped with a molecular adapter. *J Am Chem Soc* **128**, 1705-1710, doi:Doi 10.1021/Ja057123+ (2006).
- 3 Clarke, J. *et al.* Continuous base identification for single-molecule nanopore DNA sequencing. *Nat Nanotechnol* **4**, 265-270, doi:Doi 10.1038/Nnano.2009.12 (2009).
- 4 Laszlo, A. H. *et al.* Decoding long nanopore sequencing reads of natural DNA. *Nat Biotechnol* **32**, 829-833, doi:10.1038/nbt.2950 (2014).
- 5 Traversi, F. *et al.* Detecting the translocation of DNA through a nanopore using graphene nanoribbons. *Nat Nanotechnol* **8**, 939-945, doi:Doi 10.1038/Nnano.2013.240 (2013).
- 6 Kasianowicz, J. J., Brandin, E., Branton, D. & Deamer, D. W. Characterization of individual polynucleotide molecules using a membrane channel. *Proc Natl Acad Sci U S A* **93**, 13770-13773 (1996).
- 7 Venkatesan, B. M. & Bashir, R. Nanopore sensors for nucleic acid analysis. *Nat Nanotechnol* **6**, 615-624, doi:Doi 10.1038/Nnano.2011.129 (2011).
- 8 Fologea, D., Uplinger, J., Thomas, B., McNabb, D. S. & Li, J. L. Slowing DNA translocation in a solid-state nanopore. *Nano Lett* **5**, 1734-1737, doi:Doi 10.1021/NI051063o (2005).
- 9 Keyser, U. F. *et al.* Direct force measurements on DNA in a solid-state nanopore. *Nature Physics* **2**, 473-477, doi:Doi 10.1038/Nphys344 (2006).
- 10 Iqbal, S. M., Akin, D. & Bashir, R. Solid-state nanopore channels with DNA selectivity. *Nat Nanotechnol* **2**, 243-248, doi:DOI 10.1038/nnano.2007.78 (2007).
- 11 Trepagnier, E. H., Radenovic, A., Sivak, D., Geissler, P. & Liphardt, J. Controlling DNA capture and propagation through artificial nanopores. *Nano Lett* **7**, 2824-2830, doi:Doi 10.1021/NI0714334 (2007).
- 12 Wanunu, M., Sutin, J., McNally, B., Chow, A. & Meller, A. DNA translocation governed by interactions with solid-state nanopores. *Biophys J* **95**, 4716-4725, doi:10.1529/biophysj.108.140475 (2008).
- 13 Peng, H. B. & Ling, X. S. S. Reverse DNA translocation through a solid-state nanopore by magnetic tweezers. *Nanotechnology* **20**, doi:Artn 185101 Doi 10.1088/0957-4484/20/18/185101 (2009).

- 14 Huang, S. *et al.* Identifying single bases in a DNA oligomer with electron tunnelling. *Nat Nanotechnol* **5**, 868-873, doi:Doi 10.1038/Nnano.2010.213 (2010).
- 15 Yusko, E. C. *et al.* Controlling protein translocation through nanopores with bio-inspired fluid walls. *Nat Nanotechnol* **6**, 253-260, doi:10.1038/nnano.2011.12 (2011).
- 16 Di Fiori, N. *et al.* Optoelectronic control of surface charge and translocation dynamics in solid-state nanopores. *Nat Nanotechnol* **8**, 946-951, doi:10.1038/nnano.2013.221 (2013).
- 17 Krishnakumar, P. *et al.* Slowing DNA Translocation through a Nanopore Using a Functionalized Electrode. *ACS Nano* **7**, 10319-10326, doi:10.1021/nn404743f (2013).
- 18 Larkin, J. *et al.* Slow DNA Transport through Nanopores in Hafnium Oxide Membranes. *ACS Nano* **7**, 10121-10128, doi:10.1021/nn404326f (2013).
- 19 Garaj, S. *et al.* Graphene as a subnanometre trans-electrode membrane. *Nature* **467**, 190-U173, doi:Doi 10.1038/Nature09379 (2010).
- 20 Merchant, C. A. *et al.* DNA Translocation through Graphene Nanopores. *Nano Lett* **10**, 2915-2921, doi:Doi 10.1021/Nl101046t (2010).
- 21 Schneider, G. F. *et al.* DNA Translocation through Graphene Nanopores. *Nano Lett* **10**, 3163-3167, doi:Doi 10.1021/Nl102069z (2010).
- 22 Wells, D. B., Belkin, M., Comer, J. & Aksimentiev, A. Assessing Graphene Nanopores for Sequencing DNA. *Nano Lett* **12**, 4117-4123, doi:Doi 10.1021/Nl301655d (2012).
- 23 Lv, W. P., Chen, M. D. & Wu, R. A. The impact of the number of layers of a graphene nanopore on DNA translocation. *Soft Matter* **9**, 960-966, doi:Doi 10.1039/C2sm26476e (2013).
- 24 Husale, S. *et al.* ssDNA Binding Reveals the Atomic Structure of Graphene. *Langmuir* **26**, 18078-18082, doi:Doi 10.1021/La102518t (2010).
- 25 Schneider, G. F. *et al.* Tailoring the hydrophobicity of graphene for its use as nanopores for DNA translocation. *Nat Commun* **4**, doi:Artn 2619 Doi 10.1038/Ncomms3619 (2013).
- 26 Zhou, Z. *et al.* DNA Translocation through Hydrophilic Nanopore in Hexagonal Boron Nitride. *Sci Rep-Uk* **3**, doi:Artn 3287 Doi 10.1038/Srep03287 (2013).
- 27 Liu, K., Feng, J., Kis, A. & Radenovic, A. Atomically thin molybdenum disulfide nanopores with high sensitivity for DNA translocation. *ACS Nano* **8**, 2504-2511, doi:10.1021/nn406102h (2014).
- 28 Venta, K. *et al.* Differentiation of short, single-stranded DNA homopolymers in solid-state nanopores. *ACS Nano* **7**, 4629-4636, doi:10.1021/nn4014388 (2013).

- 29 Liu, X. *et al.* Top-down fabrication of sub-nanometre semiconducting nanoribbons derived from molybdenum disulfide sheets. *Nat Commun* **4**, 1776, doi:10.1038/ncomms2803 (2013).
- 30 Radisavljevic, B., Radenovic, A., Brivio, J., Giacometti, V. & Kis, A. Single-layer MoS₂ transistors. *Nat Nanotechnol* **6**, 147-150, doi:10.1038/nnano.2010.279 (2011).
- 31 Xie, P., Xiong, Q. H., Fang, Y., Qing, Q. & Lieber, C. M. Local electrical potential detection of DNA by nanowire-nanopore sensors. *Nat Nanotechnol* **7**, 119-125, doi:Doi 10.1038/Nnano.2011.217 (2012).
- 32 Farimani, A. B., Min, K. & Aluru, N. R. DNA Base Detection Using a Single-Layer MoS₂. *ACS Nano*, doi:10.1021/nn5029295 (2014).
- 33 Keskin, S., Kayrak-Talay, D., Akman, U. & Hortacsu, O. A review of ionic liquids towards supercritical fluid applications. *Journal of Supercritical Fluids* **43**, 150-180, doi:DOI 10.1016/j.supflu.2007.05.013 (2007).
- 34 Carda-Broch, S., Berthod, A. & Armstrong, D. W. Solvent properties of the 1-butyl-3-methylimidazolium hexafluorophosphate ionic liquid. *Analytical and Bioanalytical Chemistry* **375**, 191-199, doi:DOI10.1007/s00216-002-1684-1 (2003).
- 35 Khupse, N. D., Kurolkar, S. R. & Kumar, A. Temperature dependent viscosity of mixtures of ionic liquids at different compositions. *Indian Journal of Chemistry Section a-Inorganic Bio-Inorganic Physical Theoretical & Analytical Chemistry* **49**, 727-730 (2010).
- 36 Joshi, M. D. & Anderson, J. L. Recent advances of ionic liquids in separation science and mass spectrometry. *Rsc Adv* **2**, 5470-5484, doi:Doi 10.1039/C2ra20142a (2012).
- 37 Davenport, M., Rodriguez, A., Shea, K. J. & Siwy, Z. S. Squeezing Ionic Liquids through Nanopores. *Nano Lett* **9**, 2125-2128, doi:Doi 10.1021/Nl900630z (2009).
- 38 Wanunu, M., Morrison, W., Rabin, Y., Grosberg, A. Y. & Meller, A. Electrostatic focusing of unlabelled DNA into nanoscale pores using a salt gradient. *Nat Nanotechnol* **5**, 160-165, doi:Doi 10.1038/Nnano.2009.379 (2010).
- 39 Yusko, E. C., An, R. & Mayer, M. Electroosmotic flow can generate ion current rectification in nano- and micropores. *ACS Nano* **4**, 477-487, doi:10.1021/nn9013438 (2010).
- 40 Chandran, A., Ghoshdastidar, D. & Senapati, S. Groove Binding Mechanism of Ionic Liquids: A Key Factor in Long-Term Stability of DNA in Hydrated Ionic Liquids? *J Am Chem Soc* **134**, 20330-20339, doi:Doi 10.1021/0304519d (2012).
- 41 Tabard-Cossa, V., Trivedi, D., Wiggin, M., Jetha, N. N. & Marziali, A. Noise analysis and reduction in solid-state nanopores. *Nanotechnology* **18**, doi:Artn 305505

Doi 10.1088/0957-4484/18/30/305505 (2007).

42 Garaj, S., Liu, S., Golovchenko, J. A. & Branton, D. Molecule-hugging graphene nanopores. *Proc Natl Acad Sci U S A* **110**, 12192-12196, doi:DOI 10.1073/pnas.1220012110 (2013).

43 Tasserit, C., Koutsioubas, A., Lairez, D., Zalczer, G. & Clochard, M. C. Pink Noise of Ionic Conductance through Single Artificial Nanopores Revisited. *Phys Rev Lett* **105**, doi:Artn 260602

Doi 10.1103/Physrevlett.105.260602 (2010).

44 Simonsson, T. G-quadruplex DNA structures--variations on a theme. *Biol Chem* **382**, 621-628, doi:10.1515/BC.2001.073 (2001).

45 Ding, Y. H., Zhang, L., Xie, J. & Guo, R. Binding Characteristics and Molecular Mechanism of Interaction between Ionic Liquid and DNA. *J Phys Chem B* **114**, 2033-2043, doi:Doi 10.1021/Jp9104757 (2010).

46 Cardoso, L. & Micaelo, N. M. DNA molecular solvation in neat ionic liquids. *Chemphyschem* **12**, 275-277, doi:10.1002/cphc.201000645 (2011).

47 Zhang, P. F. *et al.* Ionic liquids with metal chelate anions. *Chem Commun* **48**, 2334-2336, doi:Doi 10.1039/C2cc16906a (2012).

48 Lagerqvist, J., Zwolak, M. & Di Ventra, M. Fast DNA sequencing via transverse electronic transport. *Nano Lett* **6**, 779-782, doi:Doi 10.1021/NI0601076 (2006).

49 Ohshiro, T. *et al.* Single-Molecule Electrical Random Resequencing of DNA and RNA. *Sci Rep-Uk* **2**, doi:Artn 501

Doi 10.1038/Srep00501 (2012).

Acknowledgements

We thank Prof. Jianmin Wu and Dr. Haijuan Zhang at Institute of Microanalytical System, Department of Chemistry, Zhejiang University, China for discussion in physicochemical characteristics of ionic liquids. We thank Prof. Paolo De los Rios for discussion on the force drag mechanism. We thank the Centre Interdisciplinaire de Microscopie Electronique (CIME) at EPFL for access to electron microscopes; special thanks to D. T .L. Alexander for providing training and technical assistance with TEM. Devices fabrication was partially carried out at the EPFL Center for Micro/Nanotechnology (CMi). K. L. thanks Mr. Oriol Lopez Sanchez for the training. We thank all the members from LBEN and LANES for assistance and discussion. This work was financially supported by European Research Council (grant no. 259398, PorABEL: Nanopore integrated nanoelectrodes for biomolecular manipulation and sensing and SNF Sinergia grant no. 147607). We thank Prof. Cees Dekker group and reviewers for carefully reading our manuscript and for giving detailed comments and suggestions that have been helpful to improve the manuscript.

Author contributions

J.F., K.L. and A.R. designed research. J.F., K.L. fabricated and characterized devices, performed experiments and analyzed data. R.D.B. performed single molecule fluorescence measurements, dynamic light scattering measurements and optical trapping experiments. S.K. and R.D.B. performed COMSOL modeling. D. D. performed CVD MoS₂ growth with A.K.'s supervision. J.F., K.L. A.K. and A.R. wrote the paper. All authors provided important suggestions for the experiments, discussed the results and contributed to the manuscript.

FIGURES

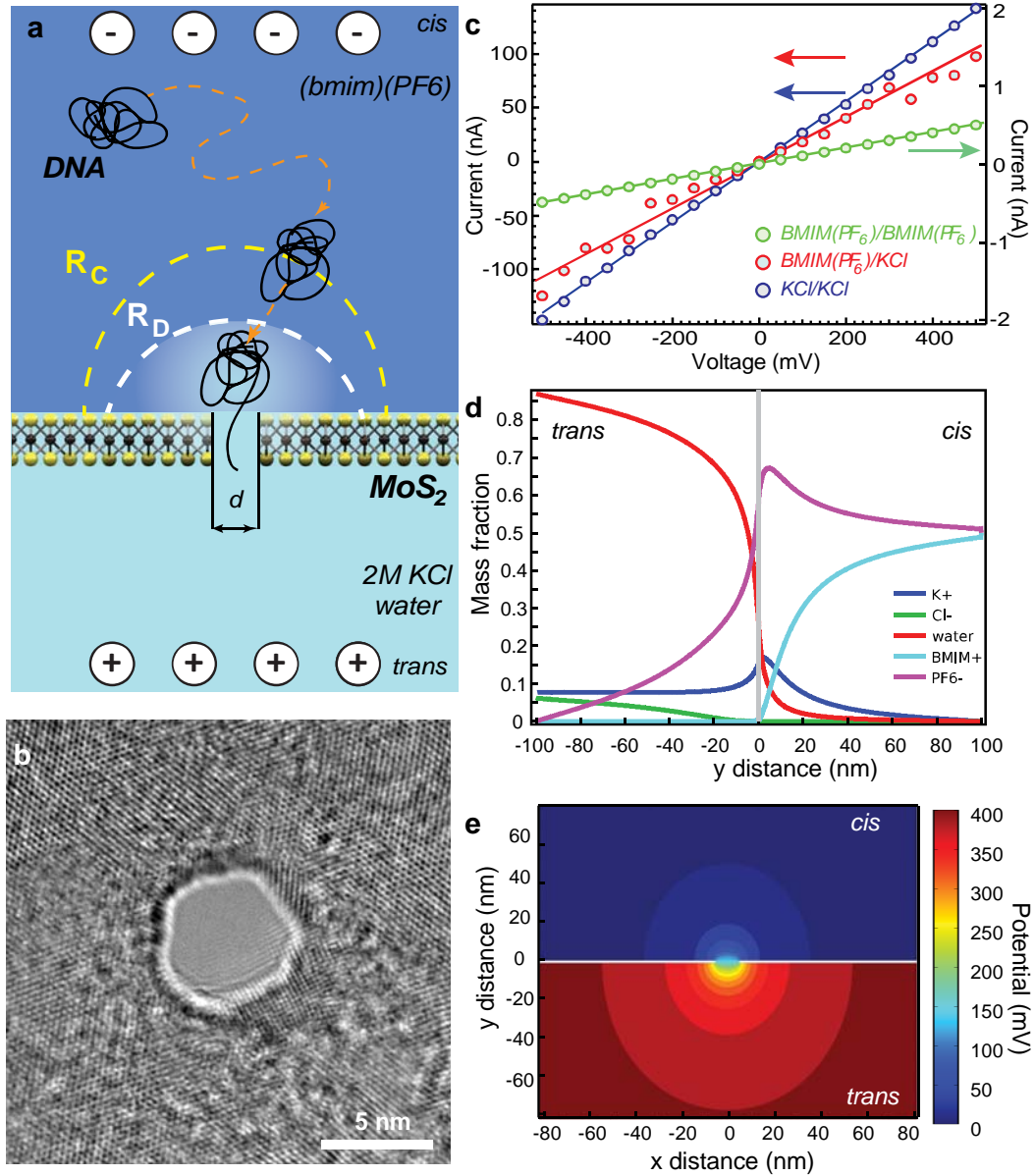


Fig. 1. Schematic and characterization of the RTILs/ KCl viscosity gradient system in a nanopores based on a 2d material. (a) *Cis* chamber contains RTILs (BmimPF₆) while *trans* chamber contains 2M aqueous KCl solution. The two chambers are separated by a monolayer MoS₂ membrane with a nanopore. Schematic also displays dynamics of DNA translocation through a monolayer MoS₂ nanopore. Away from the pore, DNA motion is purely diffusive due to the negligible electric field, but once within the area of capture radius R_c , DNA will be accelerated towards the pore by the force due to electrophoretic and electroosmotic effects. A part of DNA will undergo conformational change and one end will dive into the pore. The non-translocated part of the DNA polymer -monomers will keep the coil conformation and experience a strong Stokes dragging force from the ionic liquids. Consequently, DNA translocation

through the pore can be significantly slowed down. **(b)** Bright-field TEM image of a 5-nm solid-state pore fabricated in a monolayer MoS₂ membrane suspended over a 200 nm x 200 nm etched area formed in the center of a 20 μ m large low-stress SiN_x membrane with a thickness of being 20 nm. **(c)** Ohmic current–voltage responses of a 17 ± 2 nm MoS₂ pore. IV characteristics are taken at room temperature in a 2M aqueous KCl solution (blue circles), pure BmimPF₆ (green circles) and in BmimPF₆/2M KCl gradient (red circles) **(d)** Mass fraction of water, anions (PF₆[−] and Cl[−]), cations (Bmim⁺ and K⁺) as a function of distance from the nanopore (note that the calculation has been performed at -400 mV) **(e)** Electric potential map evaluated numerically for the viscosity gradient system shown in (a).

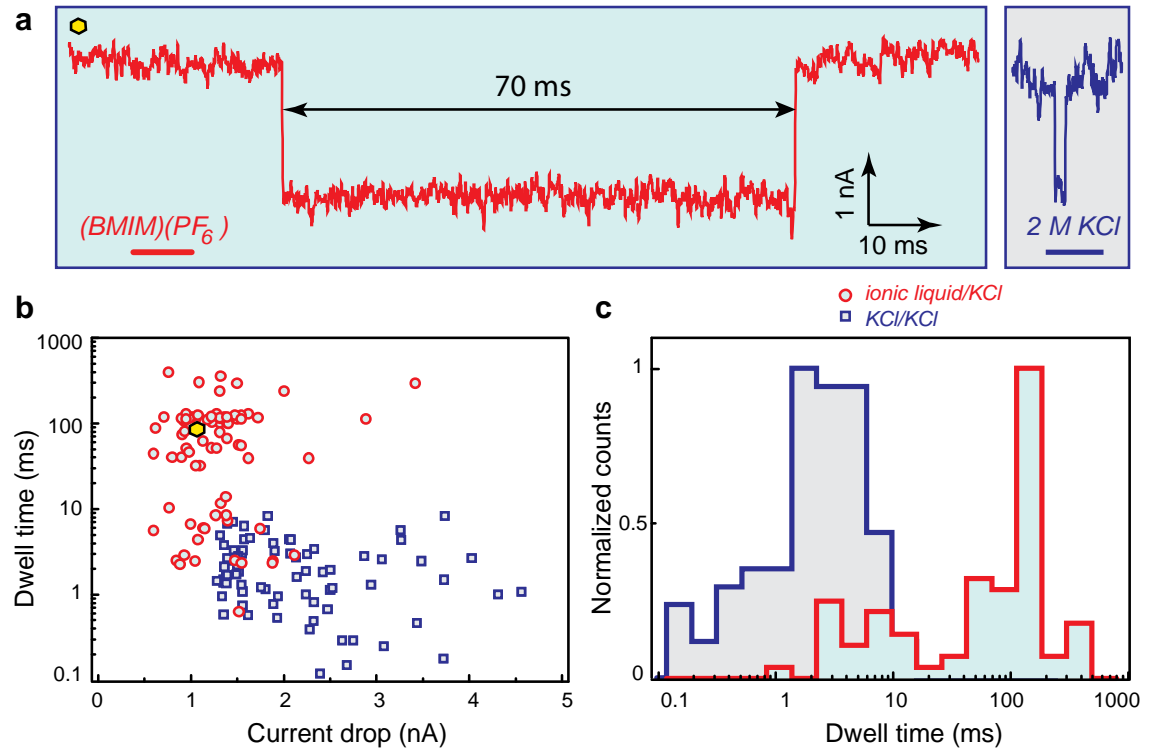


Fig. 2. Slowing down DNA translocation by increasing the electroosmotic Stokes force F_s in monolayer MoS_2 nanopore. (a) An example of a 48.5 kbp λ -dsDNA translocation event in a viscosity gradient system. The corresponding current drop represents a single DNA molecule passing through the MoS_2 pore with a diameter of 20nm. On the right, we show a typical translocation trace for 48.5 kbp λ -dsDNA obtained using the same nanopore in the absence of the viscosity gradient, resulting in translocation times that are two orders of magnitude shorter. (Displayed traces down-sampled to 10 kHz) (b) Scatter plots (blockade current versus dwell time) for dwell time versus current signal of λ -dsDNA translocation in water (blue squares), and in our viscosity gradient system (red circles) obtained using the same 20 nm diameter MoS_2 nanopore. Yellow hexagon indicates the position of the event shown in (a) in respect to other events displayed in (b) (c) Histograms of translocation times corresponding to the translocation of λ -dsDNA in water (blue) and the viscosity gradient system (red).

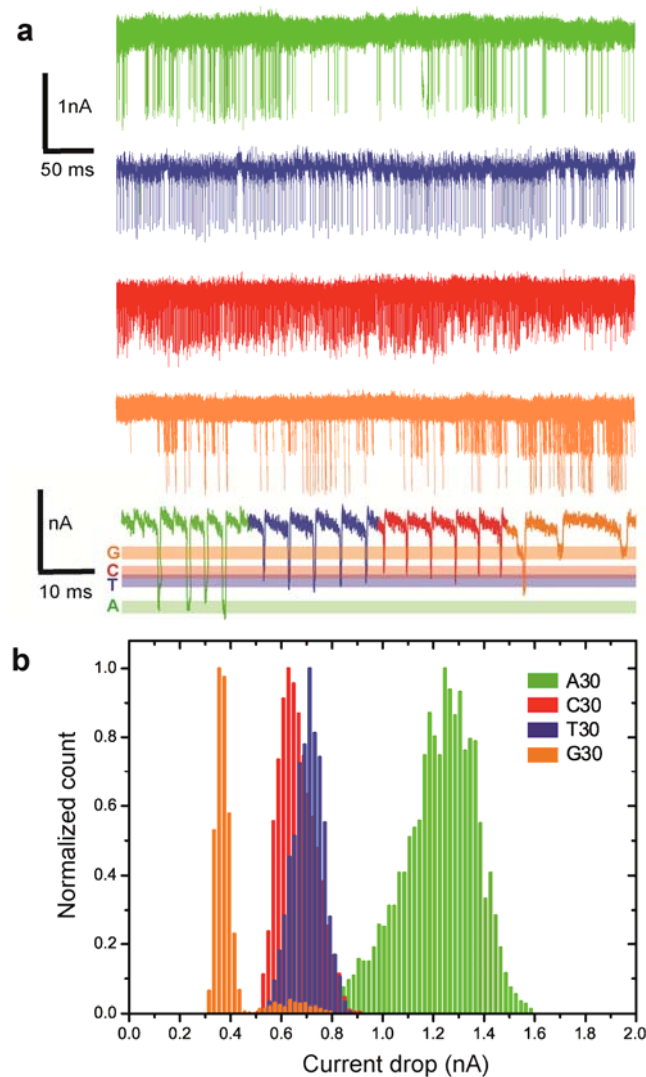


Fig. 3. Identification of four 30mer oligonucleotides in the MoS₂ nanopore. (a) 0.5 s and 0.1 s translocation signals for each homopolymer, poly A30 (green), poly C30 (red), poly T30 (blue) and poly G30 (orange). (b) Normalized histogram of current drops for each kind of the DNA homopolymer. The mean value for poly A30 is 1.25 ± 0.12 nA, for poly C30 is 0.64 ± 0.07 nA, for poly T30 is 0.71 ± 0.06 nA and for poly G30 is 0.36 ± 0.03 nA. Data acquired in pure RTIL cis chamber, 100 mM KCl, 25 mM Tris HCl, pH 7.5, trans chamber, at +200 mV. The concentration of short DNA homopolymers in RTILs is 0.02 $\mu\text{mol/ml}$.

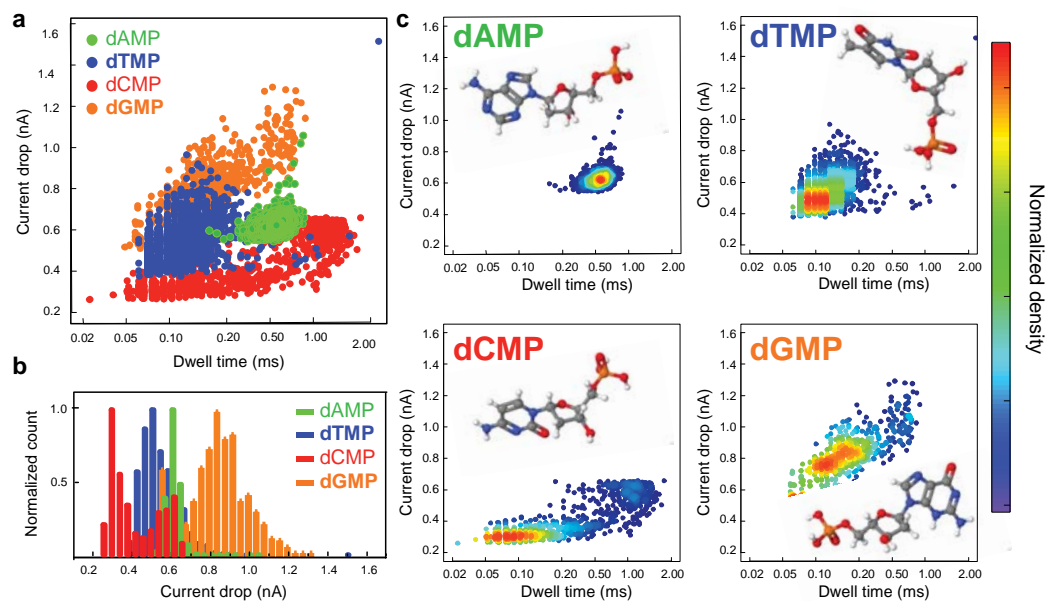


Fig. 4. Identification of single nucleotides in a MoS₂ nanopore. (a) Scatter plots of nucleotide translocation events, showing distinguished current drops and dwell times for dAMP (green), dCMP (red), dTMP (blue), and dGMP (orange). (b) Normalized histogram of current drops for dAMP, dTMP, dCMP, dGMP. (c) Density plot of single nucleotides in MoS₂ nanopore; for dAMP, the position of the hot spot is (0.5, 0.62), for dTMP, (0.09, 0.49), for dCMP, (0.06, 0.31) and for dGMP (0.15, 0.83). The color-map at the right shows the normalized density distribution of events. Data acquired in pure RTIL cis chamber, 100 mM KCl, 25 mM Tris HCl, pH 7.5, trans chamber, at +200 mV. The nucleotide concentration in RTILs was 5ug/ml. Insets show 3D models for the chemical structure of nucleotides.

Supporting Material

for

Identification of single nucleotides in MoS₂ nanopores

**Jiandong Feng^{1#}, Ke Liu^{1#}, Roman D. Bulushev¹, Sergey Khlybov¹, Dumitru
Dumcenco², Andras Kis², Aleksandra Radenovic^{1*}**

¹ *Laboratory of Nanoscale Biology, Institute of Bioengineering, School of Engineering, EPFL, 1015 Lausanne, Switzerland*

² *Laboratory of Nanoscale Electronics and Structure, Institute of Electrical Engineering, School of Engineering, EPFL, 1015 Lausanne, Switzerland*

**correspondence should be addressed to aleksandra.radenovic@epfl.ch*

equal contribution

Setup

We fabricated devices using the previously published procedure¹. Briefly, exfoliated or CVD-grown^{2,3} thin layers of MoS₂ were transferred either from SiO₂ or sapphire substrates and suspended on SiN_x membranes. Nanopores were further drilled using a JEOL 2200FS high-resolution transmission electron microscope (HRTEM) as described in Liu *et al*¹. The chips with nanopores were sealed by silicone o-rings between two polymethylmethacrylate (PMMA) chambers as reservoirs. After mounting, the entire flow cell was flushed with H₂O:ethanol (v:v, 1:1) solution and wetted for at least 30 min. This was followed by the injection of 2 M KCl solution buffered with 10mM Tris-HCl and 1mM EDTA at pH 7.0 and BminPF₆ (Aldrich-Sigma) to perform current-voltage (IV) characteristics measurements. A pair of chlorinated Ag/AgCl electrodes immersed in two reservoirs and connected to an Axopatch 200B patch clamp amplifier (Molecular Devices, Inc. Sunnyvale, CA) that was used to measure the ionic current as a function of time. Before starting experiments we adjust current offset at zero bias. The device was running at the applied voltage for at least 1 hr to perform blank experiments. DNA samples were diluted in pure BminPF₆ by mixing 10 μ L of λ -DNA stock solution with BminPF₆. DNA samples (pNEB193, plasmid 2.7 k bp, New England; λ -DNA, 48 k bp, New England) were purchased from a commercial supplier, aliquoted and stored at -20 °C before the use. Short homo polymers (Microsynth) and nucleotides (Sigma Aldrich) were purchased in dry form and directly dissolved in RTIL. We use a NI PXI-4461

card for data digitalization and custom-made LabView software for data acquisition. The sampling rate is 100 kHz and a built-in low-pass filter at 10 kHz is used. Data analysis enabling event detection is performed offline using a custom open source Matlab code, named OpenNanopore⁴ (<http://lben.epfl.ch/page-79460-en.html>). For every event, the baseline is recalculated using the average of 100 points before the start of each event. Same criteria have been used for all the compared data. CUSUM algorithm is used to fit the levels inside every event. The current drop is then calculated by subtracting corresponding averaged baseline from the level. Each type of DNA and single nucleotides were translocated in at least two different devices, and representative and reproducible results and analysis are presented.

COMSOL Modeling

Numerical calculations were performed using the COMSOL 4.2 multiphysics finite-element solver in 3D geometry, imposing a cylindrical symmetry along the axis of the nanopore. We solved the full set of Poisson–Nernst–Planck (PNP) equations, with the boundary conditions at the MoS₂ corresponding to an idealized, uncharged membrane impermeable to ions. The PNP set of equations extends Fick’s law for the case where the diffusing particles/ions are displaced with respect to the fluid by the electrostatic force. Here we have expressed particle/ion concentrations in terms of mass fractions. In particular, all ion fluxes are modeled by the Nernst-Planck equation

$$\mathbf{J}_i = -D_i \nabla c_i - \frac{Fz_i}{RT} D_i c_i \nabla \Phi \quad (1.0)$$

where \mathbf{J}_i and \mathbf{D}_i , are, respectively, the ion flux vector and diffusion coefficient of species i in the solution, T is the absolute temperature, Φ is the local potential, z_i is ionic charge and F Faraday's constant. The relationship between the net electric charge of polyelectrolyte and local average electrostatic potential is described by the Poisson's equation.

$$\nabla^2 \Phi(r) = -\frac{\rho(r)}{\varepsilon} \quad (1.1)$$

Both expressions can be rewritten using mass fractions

$$\begin{aligned} \mathbf{J}_i &= -\rho D_i^F \nabla \varpi_i + \rho \varpi_i D_i^T \frac{\nabla M_n}{M_n} + D_i^T \frac{\nabla T}{T} + \rho \varpi_i z_i \mathbf{u}_{m,i} F \nabla \Phi \\ M_n &= \left(\sum_i \frac{\varpi_i}{M_i} \right)^{-1} \end{aligned} \quad (1.2)$$

where $\varpi_i = \frac{m_i}{\sum_i m_i}$ are the mass factors, ρ is the average density, M is the molar mass

and D_i^F are diffusion and D_i^T thermal diffusion coefficients and \mathbf{u} is the fluid velocity.

In the case of 2M aqueous KCl solution (absence of the viscosity gradient), application of a fixed voltage generates the flux of K^+ and Cl^- ions that result in the net current that can be easily validated using the well-known analytical expression⁵

$$I = V \left(\left[\mu_{\text{K}^+} + \mu_{\text{Cl}^-} \right] n_{\text{KCl}} e \right) \left(\frac{4l}{\pi d^2} + \frac{1}{d} \right)^{-1} \quad (1.3)$$

where V is the applied voltage, n is the number density (proportional to concentration) of the ionic species, e is the elementary charge, and μ_{K^+} and μ_{Cl^-} are the electrophoretic mobilities of the potassium and chloride ions, respectively. Parameter d represents the pore diameter and l is the membrane thickness. In the case of the viscosity gradient, the set of PNP equations has to be solved for 5 types of diffusing

particles/ions subjected to the electrostatic force (4 ions and water molecules). Pore size was fixed to 2.5 nm, 5 nm and 10 nm (see **SI Figure1 (d-f)**). Simulated MoS₂ nanopore conductances, for all pore sizes in 2M aqueous KCl solution, viscosity gradient system or pure RT ionic liquid BminPF₆ were found to be in a good agreement with the measured values presented in **SI Figure1 (a-c)**. In the case of the pure ionic liquid condition and for a fixed voltage, the resulting current originates from the flux of the Bmim⁺ and PF₆⁻ ions.

DNA staining

DNA was stained with YOYO-1 as described elsewhere⁶. A 1 mM YOYO-1 stock solution (Invitrogen Y3601) was diluted in 10 mM sodium phosphate buffer (1.88 mM NaH₂PO₄·H₂O, 8.13 mM Na₂HPO₄·2H₂O, pH 7.5) and mixed with λ-DNA with a ratio of 1 YOYO-1 molecule for 5 base pairs.

Theoretical model

In **SI Fig. 4a** we schematize the free-energy surface with a well and a barrier to translocation for the case of our viscosity gradient system and for the 2M KCl aqueous solution. In the viscosity gradient system, λ-DNA adopts a random coil configuration with a gyration radius < 240 nm, while in the 2M KCl aqueous solution the corresponding gyration radius is ~570 nm (**SI Fig. 5**). From the schematics, it is obvious that for both systems as long as the applied voltage is lower than the free

energy barrier associated with the translocation process, one can expect low probabilities of translocations since they would only be driven by diffusion. On the other hand, increasing the applied voltage reduces the effective barrier and therefore significantly increases the probability of translocations. For the same pore, when working in the 2M KCl aqueous solution, we start to observe translocations at a much lower voltage of 100 mV compared to 200 mV when using the viscosity gradient system **SI Fig. 4b**. This figure shows the comparison between translocation times for pNEB DNA for a wide range of applied voltages and two different electrolyte systems (2M KCl in H₂O and the viscosity gradient system). According to Kramer's theory, DNA translocation governed by barrier in both systems obeys a power-law scaling,

$$\tau \sim e^{\left(\frac{\Delta G - qV}{k_B T}\right)} \quad (1.4)$$

where τ is dwell time, V the applied voltage, q effective charge and ΔG the height of the free-energy barrier. For both conditions, we observe an exponential dependence that reveals that translocation is voltage-activated, with typical events obtained at different voltages shown in **SI Fig.6**.

The Stokes drag force in the pores >5 nm

DNA-pore interactions can slow down DNA translocation in sub-5nm pores⁷, while in the larger pores those interactions are negligible. Consequently, in the pores >5nm these interactions should not contribute to the DNA retardation. In the solution,

long DNA molecules forms random coils, thus the viscous drag of the whole DNA molecule can be estimated as,

$$F_{drag} = 6\pi\eta v_{DNA} R_g \quad (1.5)$$

where R_g is the radius of gyration, η is the solvent viscosity, and v_{DNA} is the linear velocity of DNA translocation. As the polymer threads through the pore, the center of mass of this sphere moves toward the pore at a velocity:

$$v_{DNA} = \frac{dR_g}{dt} \quad (1.6)$$

Therefore, the Stokes drag force can be written as,

$$F_{drag} = 6\pi\eta_{IL} R_g \frac{dR_g}{dt} \quad (1.7)$$

If we assume that DNA translocation velocity is constant, this implies that the force balance between driving force and Stokes drag force is met at all times, *i.e.* from the first monomer translocation to the final monomer translocation.

Then, velocity can be expressed as:

$$v = \frac{R_g}{\tau} \quad (1.8)$$

where τ is the translocation time for the entire chain, denoted in experiments as the translocation dwell time. As proposed by Storm *et al.*⁸, the principal effect of hydrodynamics is to resist motion with a hydrodynamic drag (Stokes drag) on the DNA coil.

$$F_{Drag} = F_{Driving} \quad (1.9)$$

In our case with water on both sides of the nanopore,

$$qE = 6\pi\eta R_g \frac{R_g}{\tau} \quad (1.10)$$

we obtain,

$$\tau = \frac{6\pi\eta}{qE} R_g^2 \quad (1.11)$$

Due to the fractal nature of DNA polymers, the equilibrium relation between R_g , the radius of gyration of the polymer and DNA length L_0 is best described by $R_g = L^\nu$. Then the expression 1.11 for the translocation time of the entire chain can be written as

$$\tau \sim \frac{6\pi\eta}{qE} L_0^{2\nu} \quad (1.12)$$

where ν is the Flory exponent.

For our viscosity gradient system, we only consider the biggest contribution to the Stokes drag force which originates from the drag of the DNA coil in the *cis* chamber since viscosity of RTIL is much higher than water.

Then,

$$F_{drag} = 6\pi\eta_{IL} R_g^{cis} \frac{dR}{dt} \quad (1.13)$$

where

$$R_g^{cis}(t) = ((N - n)b)^\nu \quad (1.14)$$

where N is the total number of DNA monomers while n is the monomer number in the trans chamber and b corresponds to the monomer length

$$F_{drag} = 6\pi\eta_{RTIL} (N - n)^\nu b^\nu \nu b^\nu (N - n)^{\nu-1} \frac{dn}{dt} \quad (1.15)$$

Introducing the force balance,

$$qE = 6\pi\eta_{RTIL}(N-n)^v b^v v b^v (N-n)^{v-1} \frac{dn}{dt} \quad (1.16)$$

$$\int_0^\tau qE dt = \int_0^N 6\pi\eta_{RTIL}(N-n)^v b^v v b^v (N-n)^{v-1} dn \quad (1.17)$$

For the viscosity gradient system, τ_{RTIL} chain translocation time can be written

$$\tau_{RTIL} \sim \frac{3\pi\eta_{IL}L_0^{2v}}{qE} \quad (1.18)$$

At this point we can introduce a retardation factor that allows us to compare between DNA translocation well times obtained aqueous 2M KCl solution in and in the viscosity gradient system

$$r = \frac{\tau_{RTIL}}{\tau_{H_2O}} = \frac{\eta_{RTIL}}{2\eta_{H_2O}} \quad (1.19)$$

We obtain a retardation factor higher than 140 that is predominantly due to the increase in the viscosity in our viscosity gradient system.

Translocated molecules	Length (bp, nt)	Supplier
Lambda	48502	New England Biolabs
Lambda HindIII	125, 564, 2027, 2322,4361, 6557, 9416,23130	New England Biolabs
pNEB 193, plasmid	2700	New England Biolabs
poly A30, T30, G30, C30	30	Microsynth
Single nucleotides	1	Sigma

Table S1. DNA and nucleotides used in this work.

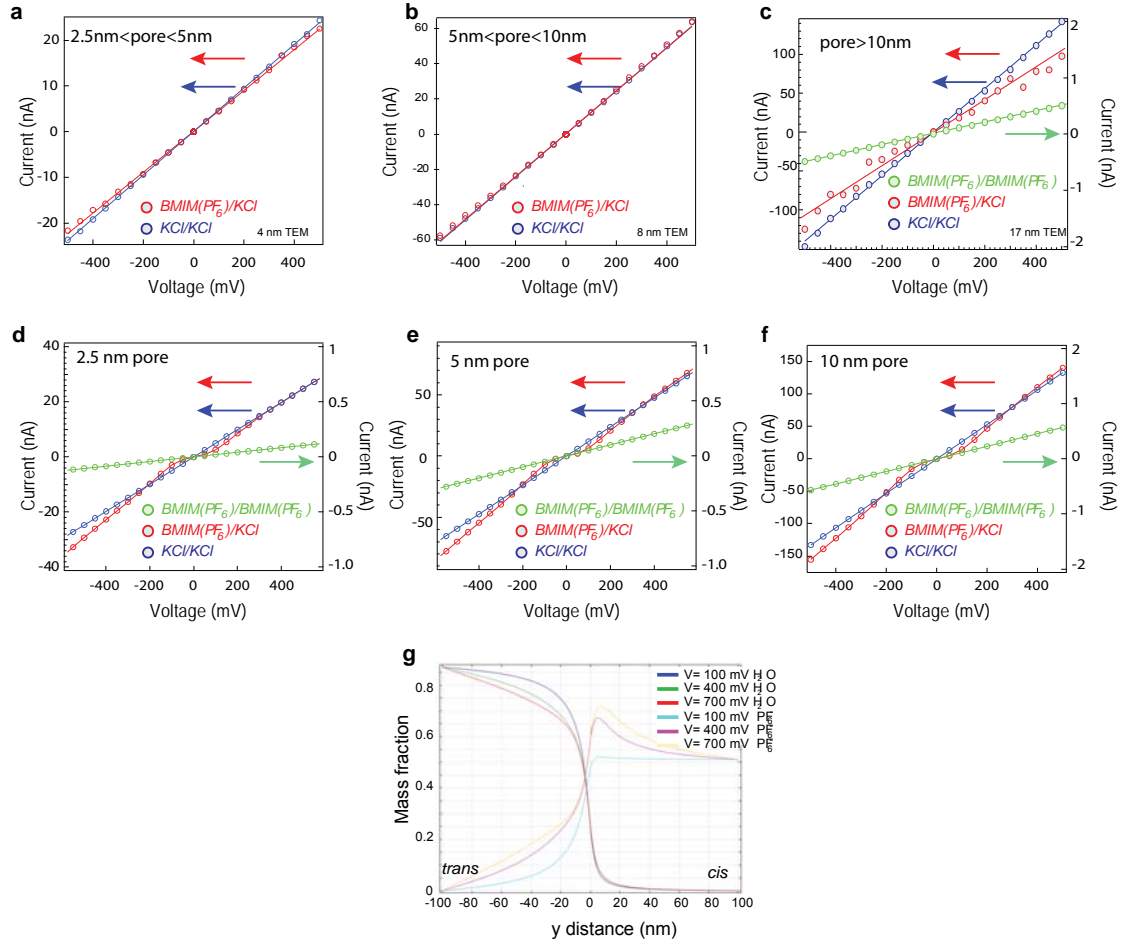
Device name	Pore size (nm)	Experiments done	Number of events	
100808A	4 ± 0.5	λ-DNA	80*	Data not shown
100718A	22 ± 2	λ-DNA	159*	Figure 2
100803B	4.7 ± 1.2	pNEB plasmid	1150	SI Figure 4 and 6
100829B	20 ± 2	pNEB plasmid	>3000	Data not shown
100619A	9.6 ± 0.8	λ-DNA and pNEB plasmid	~1100	Data not shown
100807B	8.3 ± 1	λ-Hind III digest	193*	Data not shown
100807A	4.2 ± 0.2	λ-Hind III digest	242*	Data not shown
100826B	2.5 ± 0.5	λ-Hind III digest	258*	Data not shown
100619B	6.3 ± 0.5	Poly(A) ₃₀ (T) ₃₀	~1500	Data not shown
100830B	3.7 ± 0.2	Poly(A) ₃₀ (T) ₃₀ and Poly(T) ₁₀₀	1213*	Data not shown
100913A	4 ± 1.5	Poly(A) ₃₀	100*	Data not shown
101003B	2.8 ± 0.3	Homopolymers and single nucleotides	> 10000	Figure 3 and 4
101010B	2.3 ± 0.1	dAMP, dTMP and dGMP	>3000	SI Fig 12
101014A	4 ± 0.2	dAMP, dTMP and dGMP	750*	SI Fig 12
101024B	2 ± 0.2	dAMP and dCMP	230*	SI Fig 12
101031B	2.2 ± 0.2	dAMP and dCMP	1100*	SI Fig 12
101026A	6.9 ± 0.5	dAMP and dCMP	160*	Data not shown
101102A	13 ± 3	dAMP and dCMP	350*	Data not shown
101103A	6.5 ± 0.5	dAMP and dCMP	3000*	SI Fig 12
110119A	3.3 ± 0.5	dAMP, dTMP, dCMP and dGMP	>10000	SI Fig 10,11 and 12

Table S2. List of MoS₂ nanopore devices tested under viscosity gradient conditions. In most of the nanopore devices the collection of events was stopped manually due to the increase in the noise.

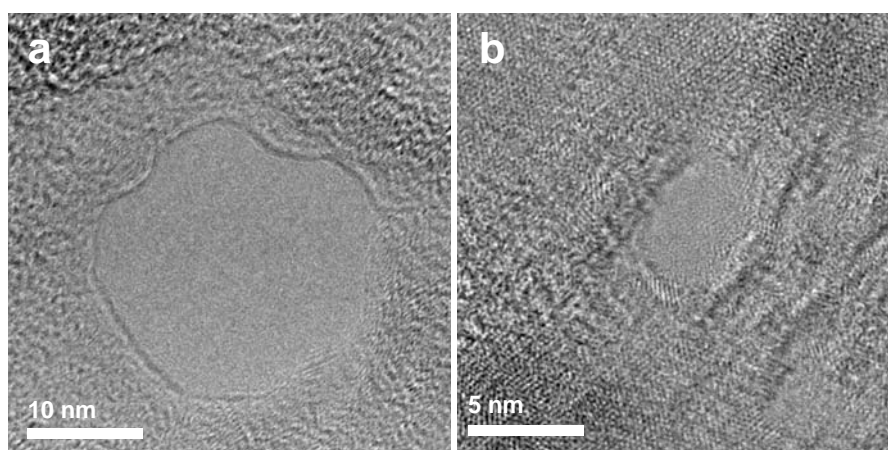
References

- 1 Liu, K., Feng, J., Kis, A. & Radenovic, A. Atomically Thin Molybdenum Disulfide Nanopores with High Sensitivity for DNA Translocation. *Acs Nano* (2014).
- 2 Najmaei, S. *et al.* Vapour phase growth and grain boundary structure of molybdenum disulphide atomic layers. *Nature Materials* **12**, 754-759, doi:10.1038/nmat3673 (2013).
- 3 van der Zande, A. M. *et al.* Grains and grain boundaries in highly crystalline monolayer molybdenum disulphide. *Nature Materials* **12**, 554-561, doi:10.1038/nmat3633 (2013).
- 4 Raillon, C., Granjon, P., Graf, M., Steinbock, L. J. & Radenovic, A. Fast and automatic processing of multi-level events in nanopore translocation experiments. *Nanoscale* **4**, 4916-4924, doi:10.1039/c2nr30951c (2012).
- 5 Wanunu, M. *et al.* Rapid electronic detection of probe-specific microRNAs using thin nanopore sensors. *Nat Nanotechnol* **5**, 807-814, doi:Doi 10.1038/Nnano.2010.202 (2010).
- 6 Carlsson, C., Jonsson, M. & Akerman, B. Double Bands in DNA Gel-Electrophoresis Caused by Bis-Intercalating Dyes. *Nucleic Acids Res* **23**, 2413-2420 (1995).
- 7 Wanunu, M., Sutin, J., McNally, B., Chow, A. & Meller, A. DNA translocation governed by interactions with solid-state nanopores. *Biophys J* **95**, 4716-4725, doi:10.1529/biophysj.108.140475 (2008).
- 8 Storm, A. J. *et al.* Fast DNA translocation through a solid-state nanopore. *Nano Lett* **5**, 1193-1197, doi:Doi 10.1021/NI048030d (2005).

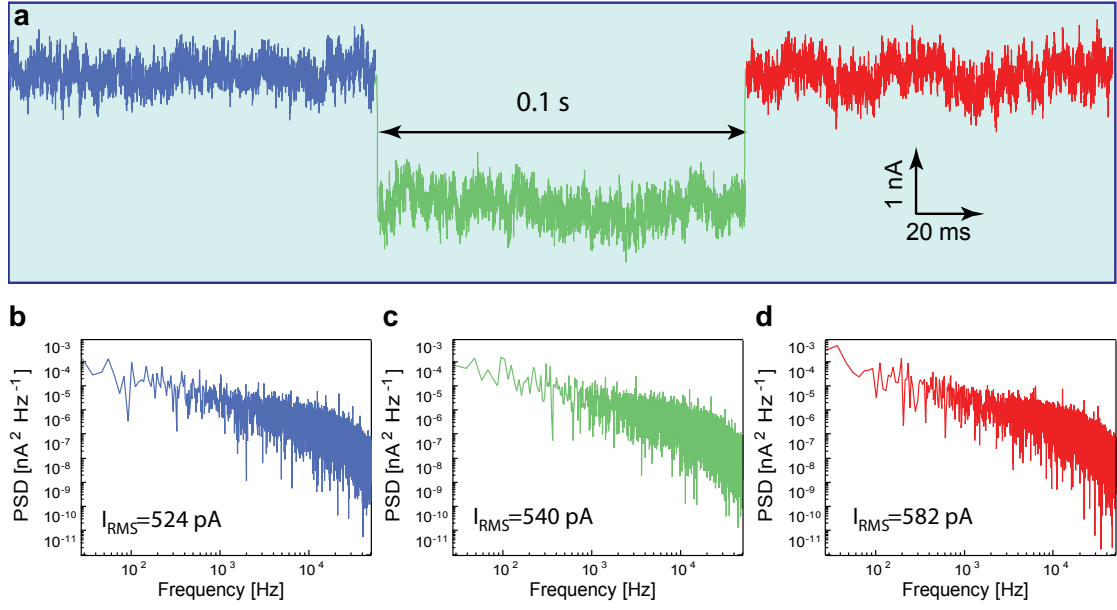
Figures



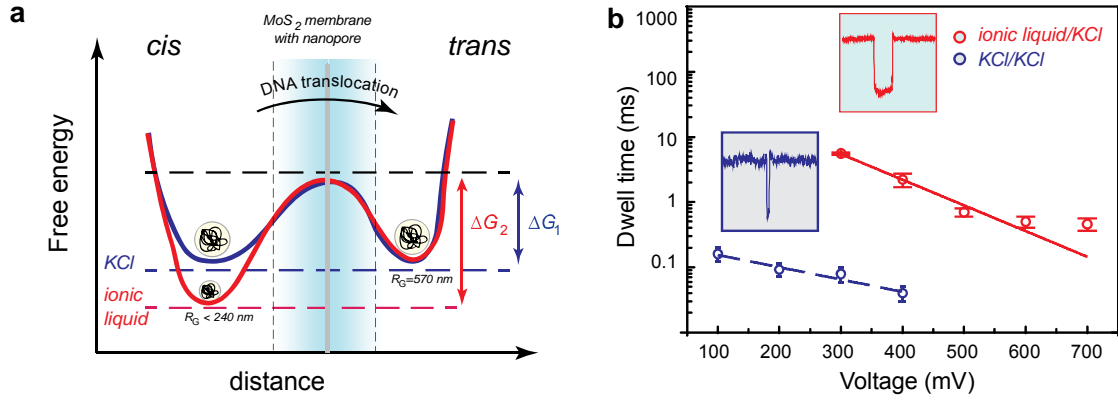
SI Fig. 1. Current-voltage characteristics of MoS₂ nanopores and COMSOL simulations of the ionic transport through a MoS₂ nanopore. Measured current–voltage characteristics for viscosity gradient system (red), pure ionic liquid (green) and 2M aqueous KCl solution (blue) (a) in a pore smaller than 5 nm (b), pore with a diameter between 5 nm and 10 nm (c) pore larger than 10 nm. Simulated current–voltage characteristics for a viscosity gradient system (red), pure ionic liquid (green) and 2M aqueous KCl solution (blue) in 2.5 nm pore having a conductance in gradient conditions of $\sim 48\text{ nS}$ (d), 5 nm pore having conductance in gradient conditions of $\sim 120\text{ nS}$ (e), and 10 nm pore having conductance in gradient conditions of $\sim 280\text{ nS}$ (f). (g) Mass fraction as a function of distance from the nanopore center (marked as 0) of water, anions (PF_6^- and Cl^-), cations (Bmim^+ and K^+) at different applied voltages.



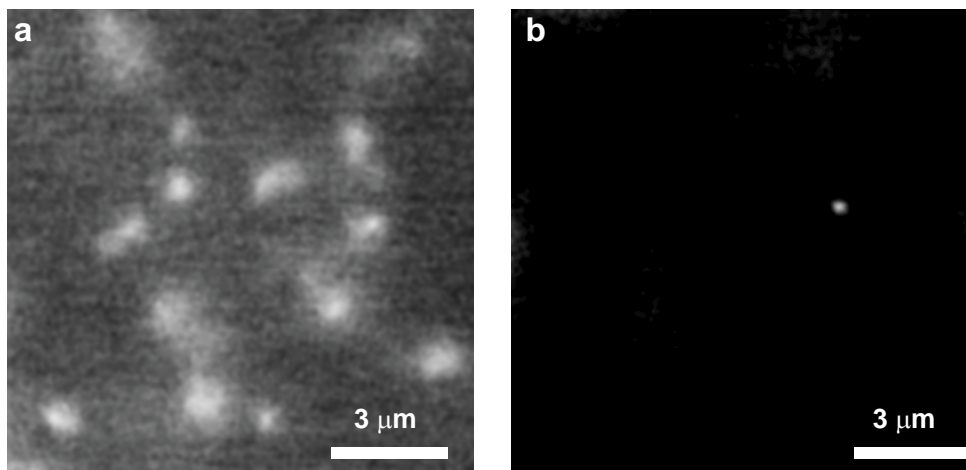
SI Fig. 2. (a) High-resolution TEM images of a 22 nm diameter MoS₂ nanopore (data shown in Fig. 2) and a 2.8 nm diameter MoS₂ nanopore (b) (data shown in Fig.3 and 4) drilled using a focused electron beam. The same pore as in (a) has been used in Liu *et.al.*¹.



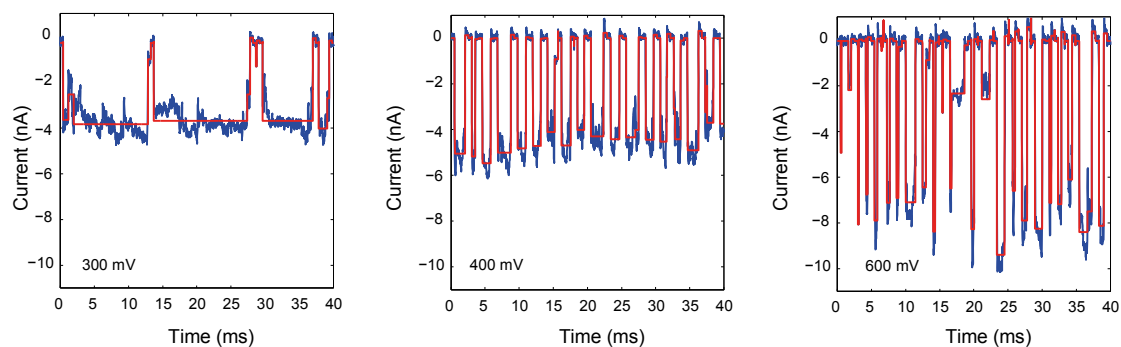
SI Fig. 3. (a) An example of a 48.5 kbp λ -dsDNA translocation event in the viscosity gradient system. Current noise power spectra for the trace presented in (a) where the noise was calculated using Welch's method from 0.1 seconds of continuous data before DNA translocation (blue (b)) during (green (c)) and after (red (d)) DNA translocation.



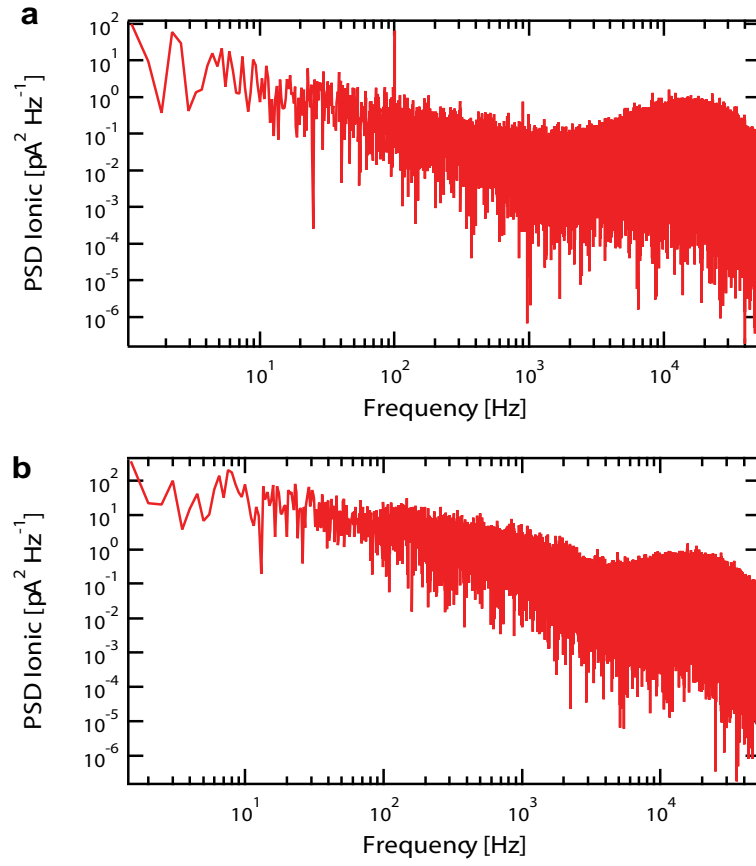
SI Fig. 4. Single molecule DNA translocation through a nanopore probes the dynamics of Kramer's theory (a) Schematic representations of single-well free-energy surfaces, for two conditions. The schematics describes the intrinsic (i.e. zero voltage) free-energy surface with a well and a barrier to translocation. In the context of the voltage-driven translocation of individual DNA molecules in a nanopore, the well of the free-energy surface corresponds to the random-coil DNA configuration in a *cis* chamber with corresponding radius of gyration, while escape over the barrier involves translocation through the nanopore and subsequent adoption of the random-coil conformation. The free energy should include at least two parts, one from the phase transfer as described using L-J equation, another from the entropy part of the DNA coil. Both of these two energy parts give a similar phase as drawn, with the only significant difference being the distance and the free-energy level. (b) Dependence of the translocation dwell time on the applied voltage for pNEB DNA in ionic liquid/ KCl solution (red) and in KCl/KCl (blue). For both conditions, we observe an exponential dependence that reveals that translocation is voltage-activated. Blue and red lines are exponential fits to the data.



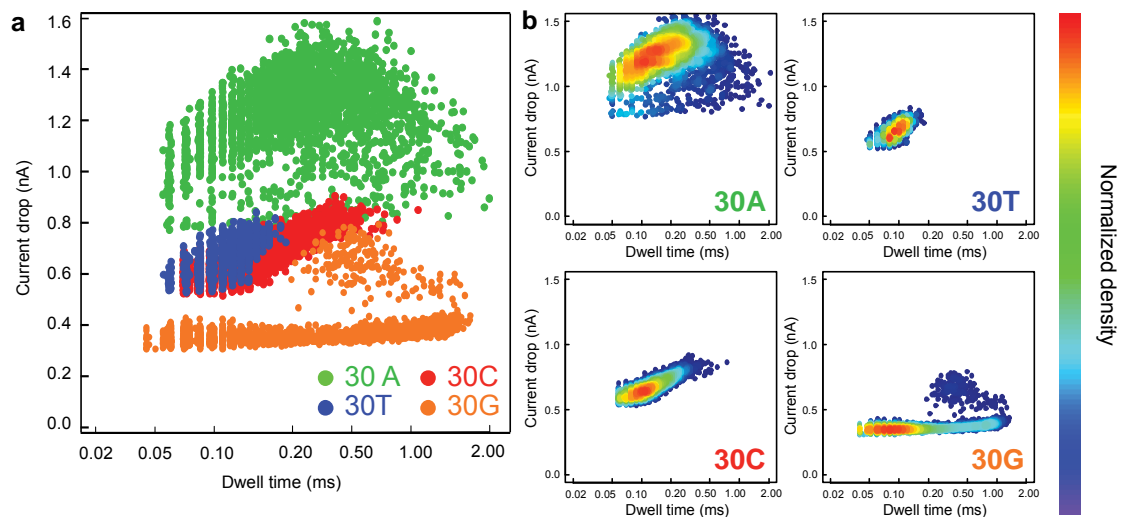
SI Fig. 5. Fluorescence images of YOYO-1 labeled λ -DNA extracted from movies used to measure the diffusion coefficient of DNA in water **(a)** and **(b)** in RTIL (BmimPF₆). By tracking the locations of individual DNA molecules through a sequence of video frames, one can measure corresponding diffusion coefficients. Same movies were used to extract radius of gyration R_g of λ -DNA. In water it was ≈ 570 nm and less than 240 nm in BmimPF₆.



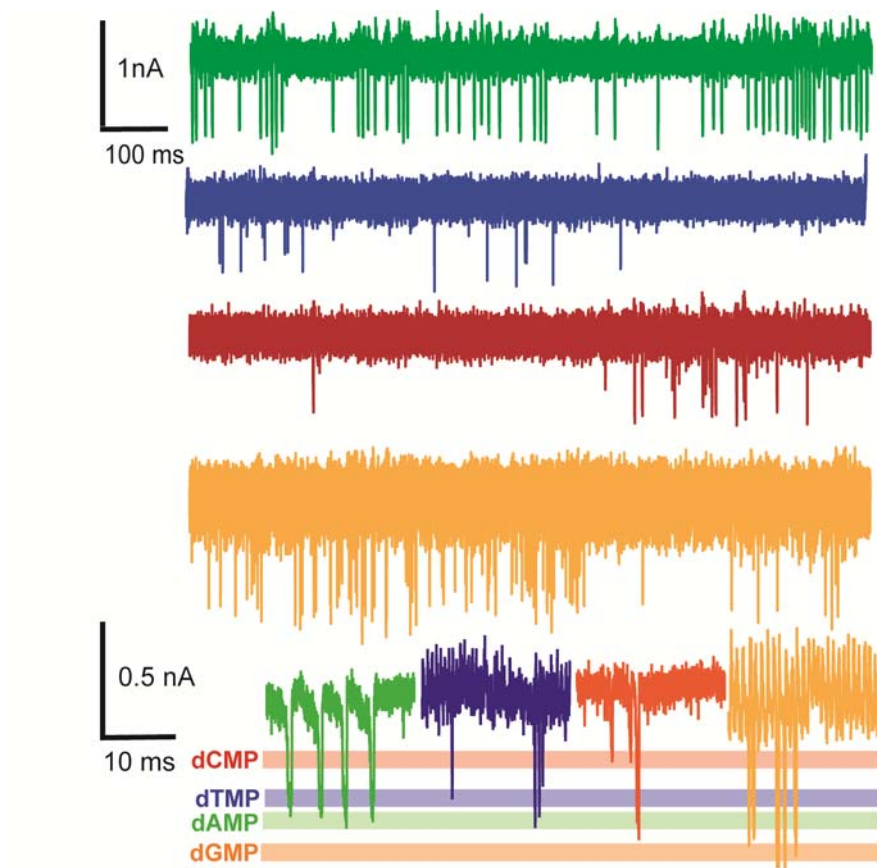
SI Fig. 6. Example traces of pNEB translocation traces through a MoS₂ pore under ionic liquid/KCl condition with variable voltages (data used for **SI Fig. 4**). The most probable dwell times, from a single-exponential fit, are 5.5 ± 0.2 ms, 2.2 ± 0.5 ms, and 0.5 ± 0.1 ms for 300 mV, 400 mV, and 600 mV, respectively. This also shows a linear relationship between the current signal and applied voltage except at 500 mV (due to baseline fluctuation). We also observed enhanced signal under viscosity gradient conditions.



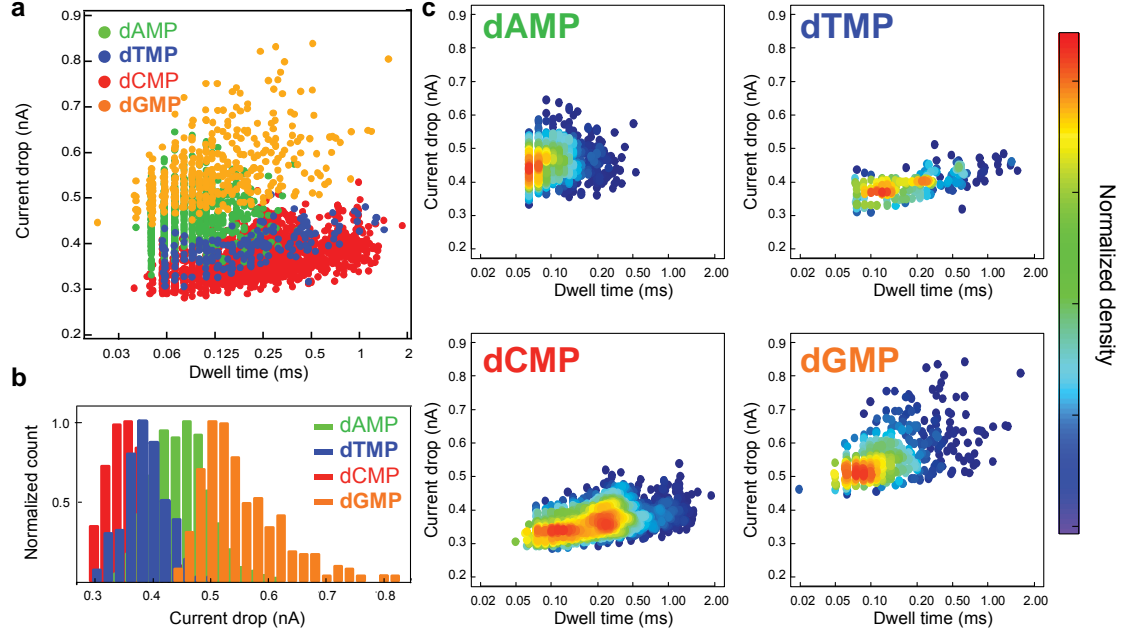
SI Fig. 7. Current noise power spectra for the 3 nm diameter MoS₂ nanopore shown in SI Figure 1b). The noise was calculated using Welch's method from 1 second of continuous data before DNA translocation (a) at 0 m bias and (b) at 200 mV.



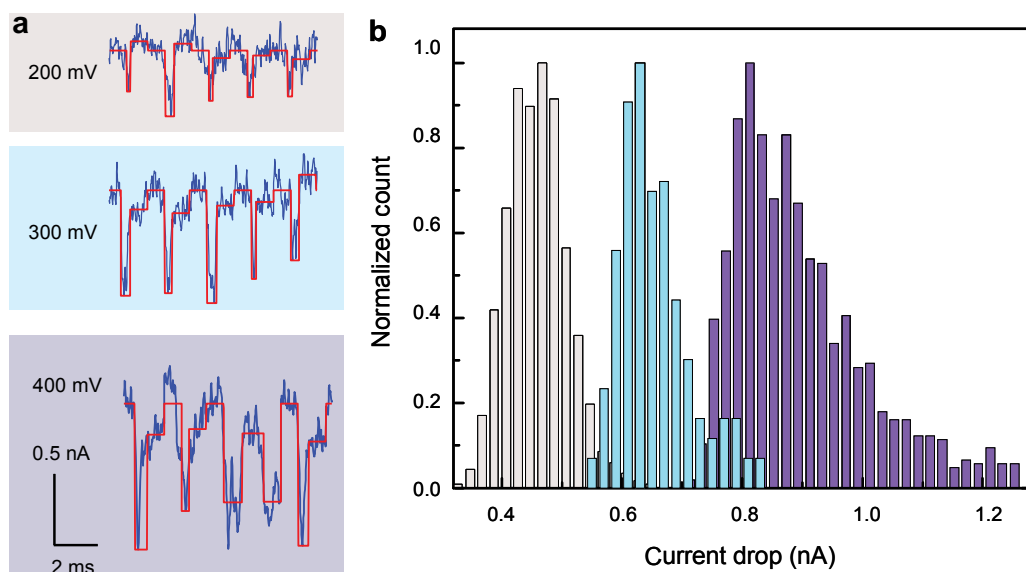
SI Fig. 8. (a) Scatter plots of nucleotide translocation, showing distinguished current drops and dwell times for poly A30 (green), poly C30 (red), poly T30 (blue), and poly G30 (orange). b) Normalized histogram of current drops for each kind of the DNA homopolymer. The mean value for poly A30 is 1.25 nA, for poly C30 is 0.65 nA, for poly T30 is 0.7nA and for poly G30 is 0.45 nA. (b) Density plots of 30mer oligonucleotides in a MoS₂ nanopore; for poly A30, the position of the hot spot is (0.15, 1.25), for poly T30, (0.1, 0.75), for poly C30, (0.12, 0.65) and for poly G30 (0.09, 0.45). The color-map on the right shows the normalized density distribution of events. Data acquired for an experimental condition of pure RTIL in the cis chamber and 100 mM KCl, 25 mM Tris HCl, pH 7.5 in the trans chamber. The bias is +200 mV. The concentration of short DNA homopolymers in RTILs is 0.02 $\mu\text{mol/ml}$.



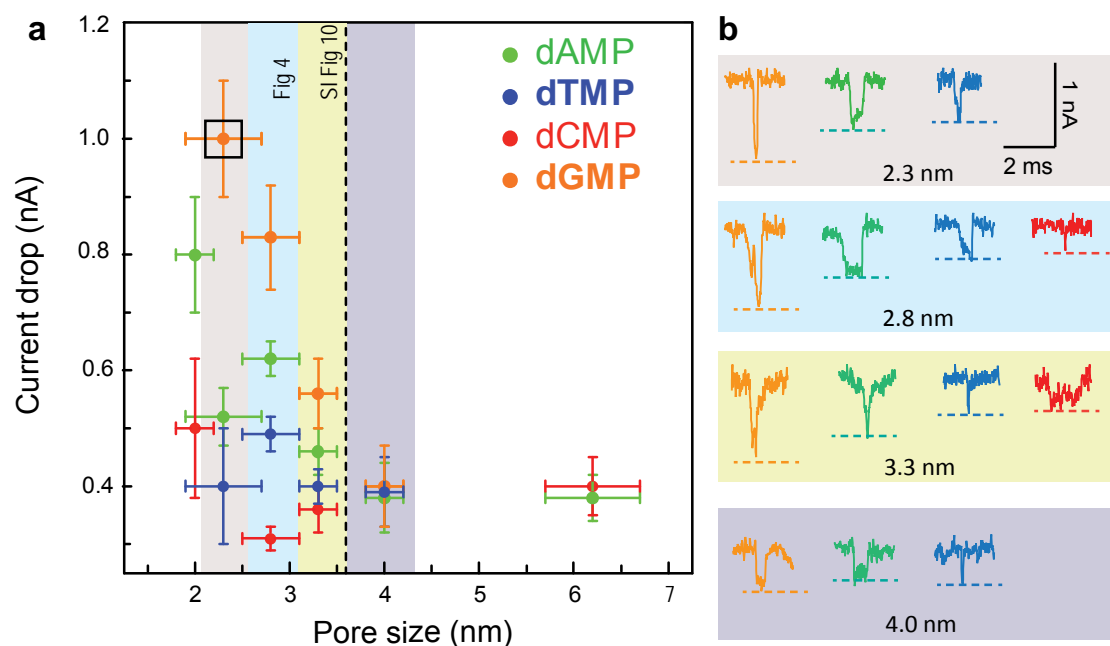
SI Fig. 9. Differentiation of single DNA nucleotides in the 2.8 nm MoS₂ nanopore under ionic liquid/KCl gradient condition. 0.5 s and 0.1 s translocation signals for each nucleotide dAMP (green), dCMP (red), dTMP (blue), and dGMP (orange).



SI Fig. 10. Identification of single nucleotides in a 3.3 nm MoS₂ nanopore. (a) Scatter plots of nucleotide translocation events, showing distinguished current drops and dwell times for dAMP (green), dCMP (red), dTMP (blue), and dGMP (orange). (b) Normalized histogram of current drops for dAMP, dTMP, dCMP, dGMP. (c) Density plot of single nucleotides in the MoS₂ nanopore; for dAMP, the position of the hot spot is (0.07, 0.46), for dTMP, (0.10, 0.40), for dCMP, (0.11, 0.36) and for dGMP (0.08, 0.56). The color-map at the right shows the normalized density distribution of events. It is clear that in the slightly larger pore nucleotide translocation events are faster and have smaller current amplitude drops. However, the trend of current drops for different types of nucleotides remains the same as shown in **Fig 4**. (dGMP>dAMP>dTMP>dCMP). Data acquired for an experimental condition of pure RTIL in the cis chamber and 100 mM KCl, 25 mM Tris HCl, pH 7.5 in the trans chamber. The bias is +200 mV. The nucleotide concentration in RTILs was 5 μg/ml.



SI Fig. 11. Example traces (a) and histograms (b) of dAMP translocation through a 3.3 nm MoS₂ pore in the presence of a viscosity gradient (ionic liquids/KCl), for different voltages (200 mV, 300mV and 400mV). The mean values for current drops are 0.46 nA, 0.65 nA, 0.91 nA, for 200 mV, 300mV, 400mV, respectively.



SI Fig. 12. Pore size dependent differentiation/identification of four nucleotides based on ionic current drops. (a) Correlation between mean current drops of four nucleotides and pore sizes. Solid circles represent the experimentally determined mean current drops (standard deviation) for dAMP (green), dCMP (red), dTMP (blue), and dGMP (orange), respectively. Errors of pore sizes originate from the asymmetry of electron beam drilled pores. The black dashed line (around 3.6 nm) represents the maximum pore size that still allows differentiating between nucleotides. Nucleotides can be statistically identified within pores smaller than the critical size that is between 3.6 and 4 nm. Black rectangle indicates the data set with highest SNR (~16). (b) Typical events related to four nucleotides (labeled in color) translocating through MoS₂ nanopores with different diameters. The levels indicate the mean values for the current drops.